

## A Study of the Sulfide Stress Corrosion Cracking in a Supermartensitic Stainless Steel by Using EIS

C.J. Ortiz-Alonso<sup>1</sup>, J.G. Gonzalez-Rodriguez<sup>1,\*</sup>, J. Uruchurtu-Chavarin<sup>1</sup>, J.G. Chacon-Nava<sup>2</sup>

<sup>1</sup> Universidad Autonoma del Estado de Morelos-CIICAP, Av. Universidad 1001, Col. Chamilpa, 62209-Cuernavaca, Mor., México

<sup>2</sup> Centro de Inv. En Materiales Avanzados, Miguel de Cervantes 108, Chihuahua, Chih., Mexico

\*E-mail: [ggonzalez@uaem.mx](mailto:ggonzalez@uaem.mx)

Received: 10 March 2015 / Accepted: 4 May 2015 / Published: 27 May 2015

---

In this work, an attempt for using electrochemical impedance spectroscopy (EIS) to study the development of sulfide stress corrosion cracking (SSCC) in a UNS S41425 supermartensitic stainless steel has been done. Slow strain rate tests have been used to achieve this goal. It was found that when the steel is susceptible to SSCC, both the Bode modulus and phase angle decreased as straining increased between 0.1 and 10 Hz. Electric circuit was used to simulate the EIS data and it was found that both the diffusion layer resistance inside and the crack charge transfer resistance decreased after the yielding point.

---

**Keywords:** Corrosion cracking, stainless steel, electrochemical impedance spectroscopy.

### 1. INTRODUCTION

Stress corrosion cracking (SCC) is a type of failure that causes many accidents and high economical losses in the industry [1] and when it is caused by sulfide present in the environment, it is named sulfide stress corrosion cracking (SSCC). Sulfide is present in a great quantity of pipelines and oilfield equipment are required for the operation of oil and gas fields, making them highly susceptible to SSCC [2-5]. Normally, in sulfide-containing environments, 13%Cr martensitic stainless steels and 22 or 25%Cr duplex stainless steels were used. The corrosion resistance of stainless steels increases with increasing the contents of Cr whereas other elements are involved to stabilize the passive film (Mo, Ni, N, Cu, Co, Ti, W), giving rise to special alloys called Corrosion Resistance Alloy (CRA) - such as martensitic and supermartensitic stainless steels [6]. Due to their good corrosion resistance and mechanical properties, martensitic stainless steels have been increasingly applied in oil and gas

application [7,8]. Generally they are used in several corrosion conditions and when economical aspects are a critical issue, since they offer better mechanical and corrosion properties than carbon steels [9-12].

Electrochemical techniques such as electrochemical noise (EN), which is a non-destructive technique, has been extensively used to detect stress corrosion cracking susceptibility of metallic alloys in different environments [13-23], obtaining current or potential fluctuations and were related with the nucleation and propagation of stress corrosion cracks. However, the use of Electrochemical Impedance Spectroscopy (EIS) measurements in the study of SCC has been more limited. For instance, Oskuie [24] used EIS to study the susceptibility to SCC of a X-70 pipeline steels with the aid of a widely used technique called Slow strain rate testing (SSRT) in a solution containing high pH bicarbonate. EIS tests at a fixed potential were conducted simultaneously at regular periods of time in order to elucidate the changes associated with the SCC. Both type of Bode for cracks were calculated. They found the range of a suitable frequency were the detection of cracks. Bosh [25] applied the EIS technique in the monitoring SCC in a stainless steel sample exposed to a high temperature aqueous environment. The impedance of a cracked surface was described with a model which could distinguish between a flat electrode surface and an electrode surface with cracks. They used three types of experiments: (1) Sensitized Type 304 SS by using Slow strain rate tests on in a 5 N H<sub>2</sub>SO<sub>4</sub> + 0.1 M NaCl solution, (2) 304 type stainless steel by using the constant load tests in a boiling ( $\pm 110$  °C) acidified sodium chloride solution, and (3) 304 type stainless steel with the aid of the slow strain rate tests in an oxygen containing solution of 0.01 M Na<sub>2</sub>SO<sub>4</sub> at 300 °C. the phase shift between the two samples could be related to the stress corrosion cracking process. Lou [26] used slow strain rate tests applied EIS measurements in order to study the susceptibility of carbon steel to SCC in simulated fuel-grade ethanol (SFGE). They found that the Phase angle decreased during an active crack growth. When the steel was susceptible to SCC, the frequency at maximum phase angle increased around 1 Hz. Thus, the goal of this paper is to use EIS measurements to detect SSCC of a supermartensitic stainless steel in an H<sub>2</sub>S-containing environment.

## 2. EXPERIMENTAL PROCEDURE

**Table 1.** Chemical composition of tested steel. (wt. %).

C	Mn	Si	Cr	Ni	Mo	S	P	Cu	N	Fe
0.02	0.75	0.3	13.5	4.7	1.7	0.0003	0.016	0.07	0.07	Bal.

Tested material included a supermartensitic stainless steel, UNS S41425, with chemical composition as given in table 1. Steel was austenitized at 932 °C during 60 min, air cooled, tempered at 611 °C during 11 hours and air cooled. Cylindrical tensile specimens with a 25.00 mm gauge length and 2.50 mm gauge diameter were machined. Before testing, the specimens were abraded longitudinally with 600-grade emery paper, degreased, and masked, with the exception of the gauge length. The employed technique to assess the susceptibility to SCC was slow strain rate tensile (SSRT)

testing at a strain rate of  $1.00 \times 10^{-6} \text{ s}^{-1}$ . Testing solution includes a heated, de-aerated 3% NaCl solution, whereas  $\text{H}_2\text{S}$  was produced by reacting  $3.53 \text{ mg L}^{-1}$  Sodium Sulfide ( $\text{Na}_2\text{S}$ ) with  $1.7 \text{ mg L}^{-1}$  Acetic acid at 25, 40, 60 and  $80 \text{ }^\circ\text{C}$ . SCC tests were carried out at the free corrosion potential value. The susceptibility to SCC was measured by the loss in ductility in terms of the percentage reduction in area (%R.A) with the aid of following equation:

$$\%R.A. = \frac{A_i - A_f}{A_i} \times 100 \quad [1]$$

where  $A_i$  and  $A_f$  are the initial and final area respectively. A susceptibility index to SCC ( $I_{\text{SCC}}$ ) was calculated as follows:

$$I_{\text{SCC}} = \frac{\%R.A._{\text{air}} - \%R.A._{\text{NACE}}}{\%R.A._{\text{air}}} \quad [2]$$

where  $\%RA_{\text{air}}$  and  $\%RA_{\text{NACE}}$  are the percentage reduction in area values in air and in the NACE solution respectively. A value of  $I_{\text{SCC}}$  close to 0 means immunity towards SCC, whereas a value close to 1 indicates a high susceptibility. Tensile-fractured specimens were examined by a JEOL scanning electron microscope (SEM). EIS tests were carried out at the  $E_{\text{corr}}$  value during the straining by using a signal with amplitude of  $10 \text{ mV}_{\text{SCE}}$  and a frequency interval of  $0.1 \text{ Hz}$ - $30 \text{ kHz}$  by using a PC4 300 Gamry potentiostat. Measurements were obtained during straining by using a graphite rod as auxiliary electrode, a saturated calomel electrode (SCE) reference electrode with a Luggin capillary bridge. Polarization curves were performed in a potentiodynamic way at a sweep rate of  $1 \text{ mV s}^{-1}$  in an AC Gill potentiostat once the free corrosion potential value ( $E_{\text{corr}}$ ) was stable. A saturated calomel reference electrode (SCE) was used as reference electrode whereas a graphite rod was the auxiliary electrode. Cylindrical specimens were encapsulated in commercial epoxic resin with a total exposed area of  $1.0 \text{ cm}^2$ . Potentiodynamic polarization curves were performed. Corrosion current values,  $I_{\text{corr}}$ , were calculated by using Tafel extrapolation method.

### 3. RESULTS AND DISCUSSION

The effect of the temperature in the polarization curves is shown in Fig. 1, where it can be seen that at room temperature, i.e.  $25 \text{ }^\circ\text{C}$ , the steel displayed an active-passive behaviour with an  $E_{\text{corr}}$  value around  $-755 \text{ mV}_{\text{SCE}}$  and an  $I_{\text{corr}}$  value close to  $0.002 \text{ mA cm}^{-2}$ . The passive zone started around  $-700 \text{ mV}_{\text{SCE}}$  and ended at a pitting potential value close to  $-200 \text{ mV}_{\text{SCE}}$  after which a transpassive zone could be found. When the temperature increases up to 60 or  $80 \text{ }^\circ\text{C}$ , the  $E_{\text{corr}}$  values increased up to  $-590$  and  $-550 \text{ mV}_{\text{SCE}}$  respectively whereas the  $I_{\text{corr}}$  was very similar for both temperatures, close to  $0.1 \text{ mA cm}^{-2}$ , but the steel still displayed an active-passive behaviour. The passive zone was narrower than that found at  $25 \text{ }^\circ\text{C}$ , but the pitting potential remained the same at the three different temperatures. It has been reported that in  $\text{H}_2\text{S}$ -containing solutions, the corrosion process of iron and steel is generally accompanied by iron sulfide film formation [27-30] such as mackinawite, cubic FeS, troilite, and pyrite, which are porous, non-protective. However, the presence of Cr, Ni and probably Mo could

make these films more protective than those found on iron or steels. The addition of Mo improves the pitting resistance and enhances passivity.

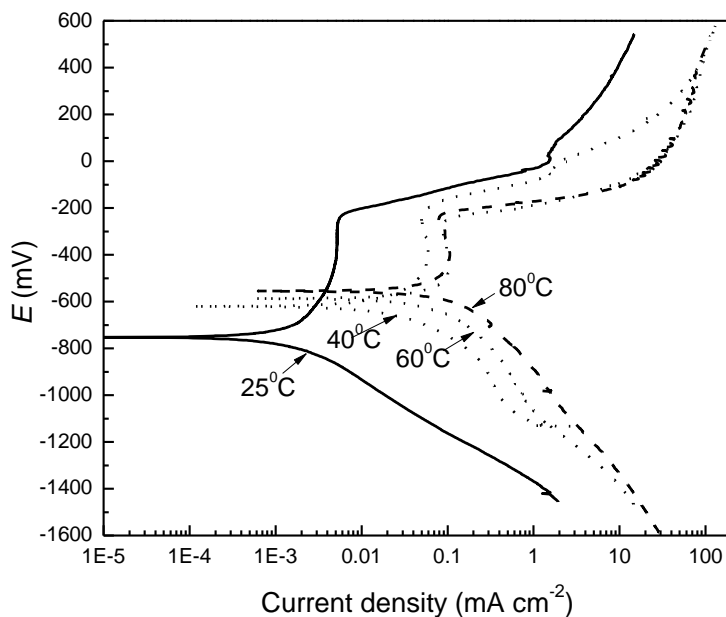


**Figure 1.** Effect of the temperature in the polarization curves for UNS S41425 supermartensitic stainless steel in H<sub>2</sub>S-containing 3.5 % NaCl solution.

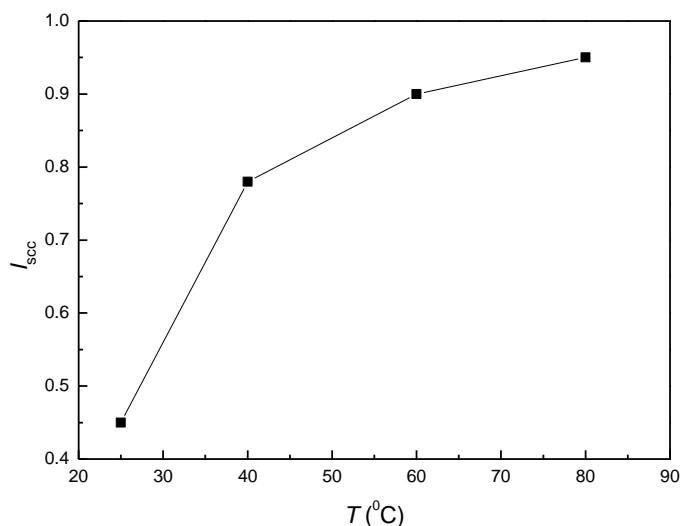


**Figure 2.** Effect of the temperature in  $I_{sec}$  value for UNS S41425 supermartensitic stainless steel in H<sub>2</sub>S-containing 3.5 % NaCl solution.

This is so for several factors which produce a passive film more resistant, making easier the transition from an active-to-passive behavior by reducing the anodic peak, and slowing down the

dissolution rate for the naked substrate making it more difficult to sustain the local chemistry necessary for localized corrosion. By combining Mo with Ni, the outer layers of the passive film has been shown [31] to be enriched whereas the inner passive layer is made of Cr. Additionally, Mo is considered to form MoS giving protectiveness in presence of H<sub>2</sub>S. This stops the access of H<sub>2</sub>S to the under-layer, consisting of solely chromium oxide. The formed films become more porous and less protective with an increase in the temperature and thus, it will occur an increase in the corrosion rate.

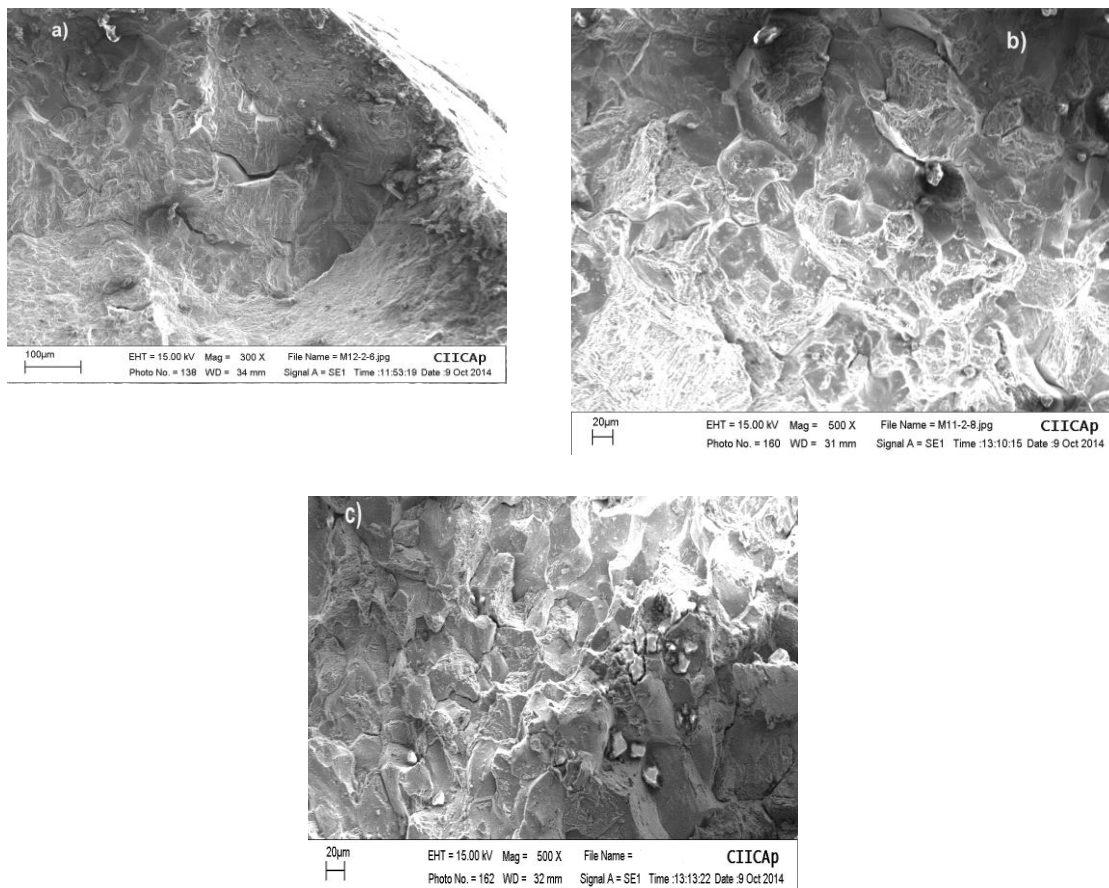


**Figure 3.** Micrographs of specimens fractured in a H<sub>2</sub>S-containing 3.5 % NaCl solution at a) 25, b)60 and 80°C.

The susceptibility towards SCC for the a supermartensitic stainless steel in the H<sub>2</sub>S-containing NaCl solution is given in Fig. 2, where it can be seen that the steel is practically immune to SCC at 25 °C but it is very susceptible to SCC as the temperature increases. This was confirmed by micrographs of fractured specimens shown in Fig. 3, were it can be seen that as the testing temperature increases, the specimens showed a brittle type of fracture, with some quasicleavage features and intergranular type of cracking. Although stress-strain curves were not performed, Salazar et al. [32] did with a supermartensitic stainless steel very similar in both chemical composition and mechanical properties. Both in air and in synthetic sea water the yielding point was reached within 8 h, whereas the UTS was reached around 24 h, thus, by comparing both results, it can be known in which point of the stress-strain curves the EIS readings were taken.

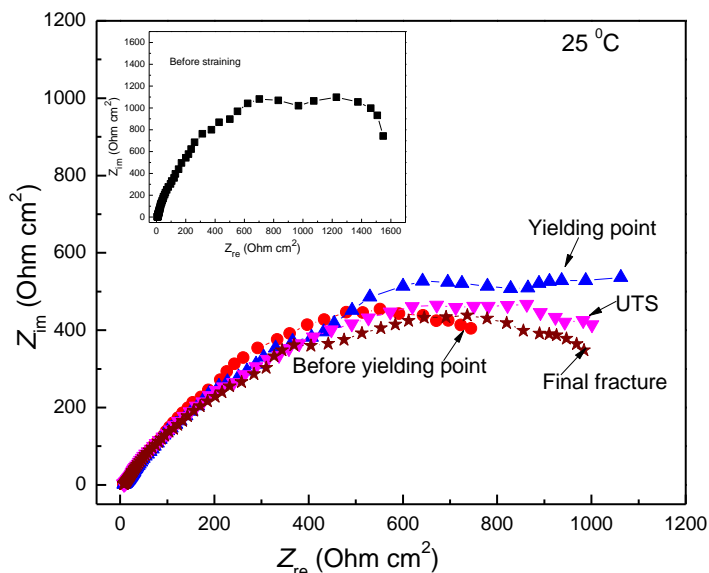


**Figure 4.** Nyquist curve for UNS S41425 supermartensitic stainless steel in  $\text{H}_2\text{S}$ -containing 3.5 % NaCl solution at  $25^\circ\text{C}$  during the SSRT.

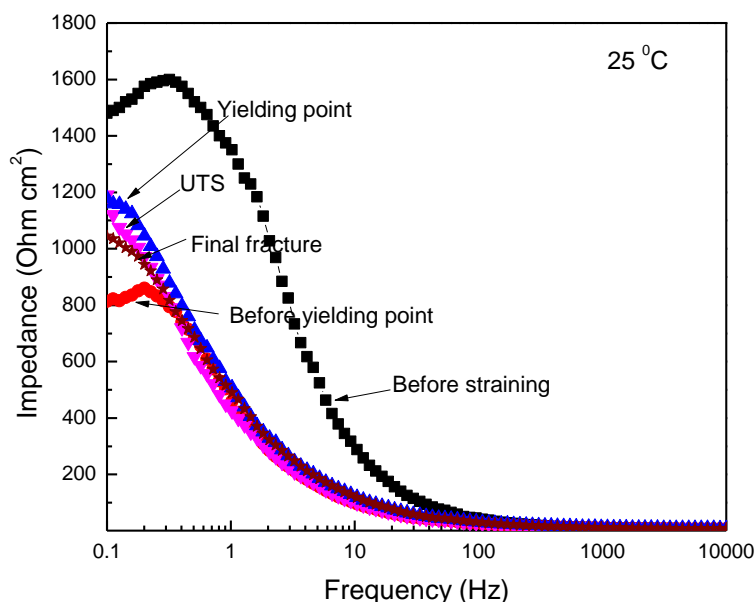


**Figure 5.** Bode plot in the Impedance-frequency format for UNS S41425 supermartensitic stainless steel in  $\text{H}_2\text{S}$ -containing 3.5 % NaCl solution at  $25^\circ\text{C}$  during the SSRT.

Nyquist diagram for specimen fractured at  $25^\circ\text{C}$ , which was immune to SCC, is shown in Fig. 4, where it can be seen that, before applying any stress, data displayed two semicircles: one at high and intermediate frequency values, and another one at lower frequencies, indicating a corrosion process controlled by the charge transfer reaction. As stated above, in  $\text{H}_2\text{S}$ -containing solutions, the corrosion process of iron and steel is generally accompanied by the formation of iron sulfide film. Thus, one of the observed loops in Fig. 4 corresponds to the formed sulfide film, whereas the second loop

corresponds to the double electrochemical layer. As soon as the straining started, the two observed semicircles remained throughout the tests, but their diameters decreased as compared to the unstrained specimen. During the first hours of testing and before reaching the yielding point, the semicircles diameter increased due to film growth due to corrosion activity. After the yielding point, the semicircles diameter decreased until the final fracture, due to the deterioration of the film. Bode plot in the Modulus format, Fig. 5, showed that the modulus was higher for the unstressed condition, and it decreased when the straining begun, diminishing as the strained continued throughout the test, confirmed by the Nyquist results, indicating that the growth of the external formed sulfide film is affected by the straining.

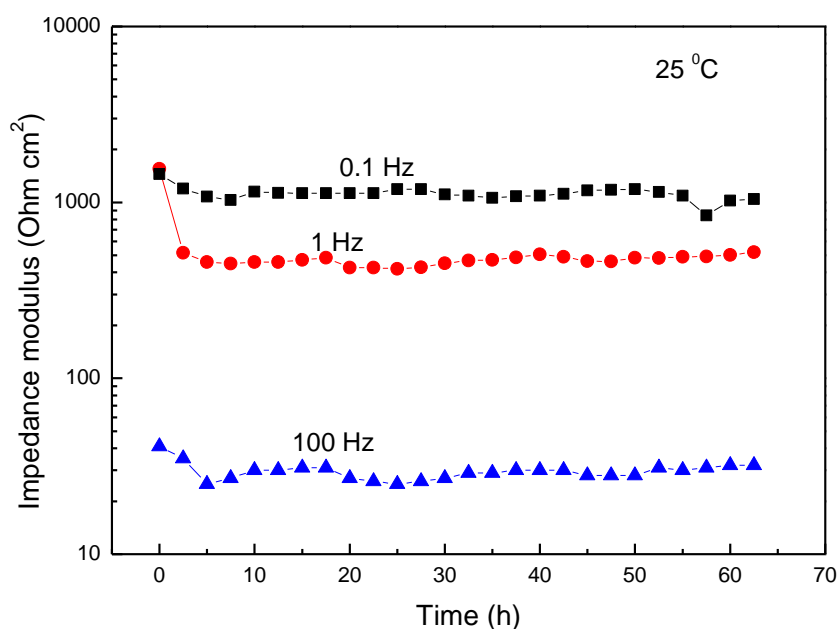


**Figure 6.** Evolution of the impedance modulus with time at different frequency values for UNS S41425 supermartensitic stainless steel in H<sub>2</sub>S-containing 3.5 % NaCl solution at 25 °C during the SSRT.

The evolution of the impedance modulus with time at different frequency values (0.1, 1 and 100 Hz) is shown in Fig. 6, where it can be seen that, generally speaking, the impedance value increased as the frequency decreased and, at the same frequency value, it remained more or less constant as time increased. On the other hand, Fig. 7 shows that before applying any stress, the phase angle increased as the frequency decreased, remaining more or less constant between 100 and 0.1 Hz, where it started to decrease with a further decrease in the frequency.

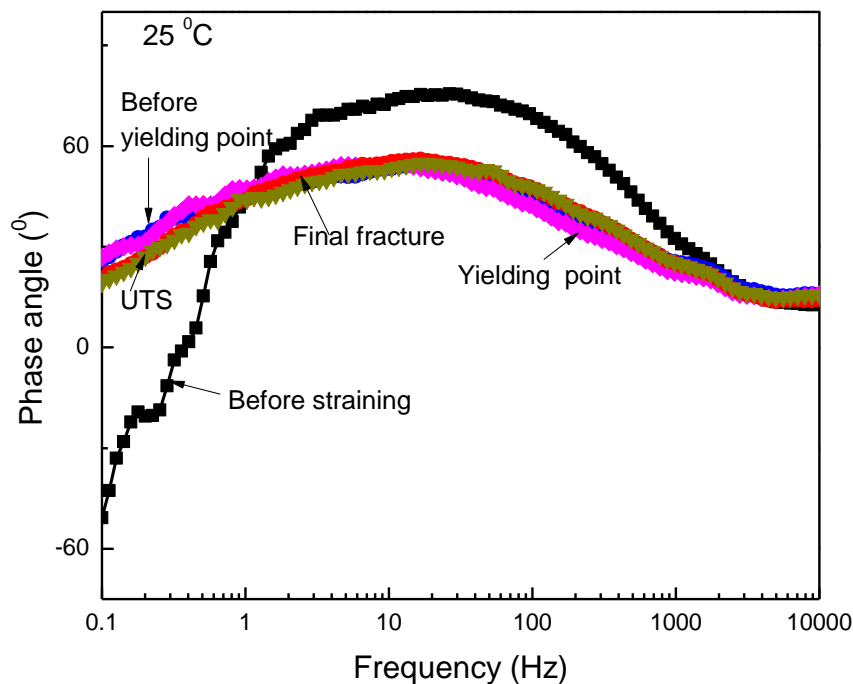


**Figure 7.** Bode curve in the Phase angle-frequency format for UNS S41425 supermartensitic stainless steel in H<sub>2</sub>S-containing 3.5 % NaCl solution at 25 °C during the SSRT.

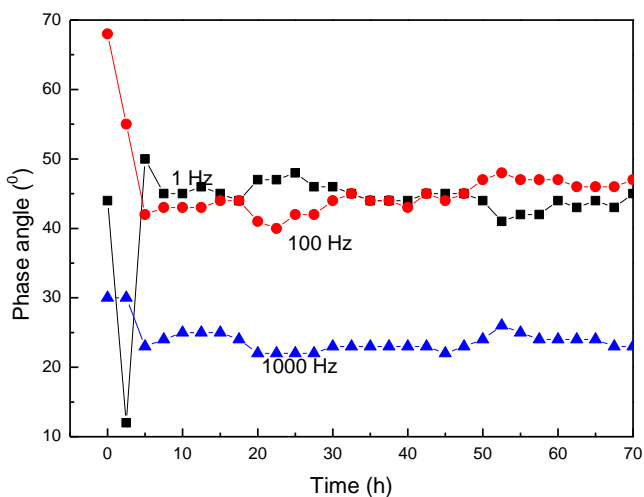


**Figure 8.** Evolution of the phase angle with time at different frequency values for UNS S41425 supermartensitic stainless steel in H<sub>2</sub>S-containing 3.5 % NaCl solution at 25 °C during the SSRT.

As the straining started, the phase angle was lower than that for the unstressed condition at frequency values higher than 1 Hz; below this frequency, the phase angle values were higher than those in the unstressed condition. For the stressed condition, the phase angle values were virtually the

same regardless of the deformation of the steel. This is confirmed in Fig. 8, which shows the evolution of the phase angle with time at different frequency values. This figure shows that at the same frequency, although there is a decrease in the phase angle during the first hours of straining, it remained more or less constant as time elapsed until the specimen reached its final fracture.

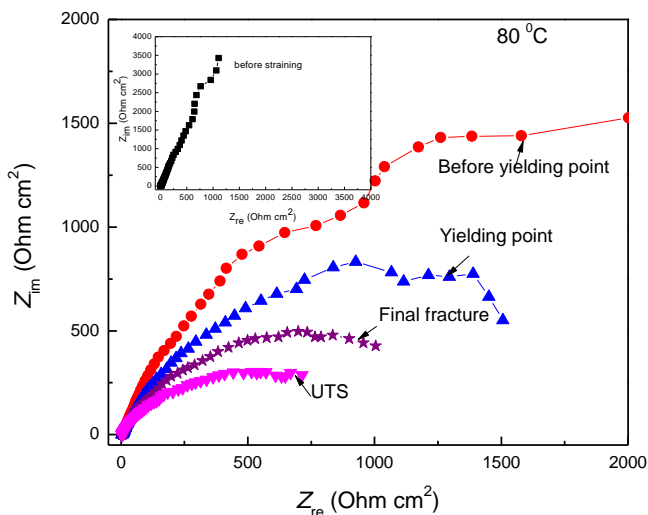


**Figure 9.** Nyquist curve for UNS S41425 supermartensitic stainless steel in H<sub>2</sub>S-containing 3.5 % NaCl solution at 80 °C during the SSRT.

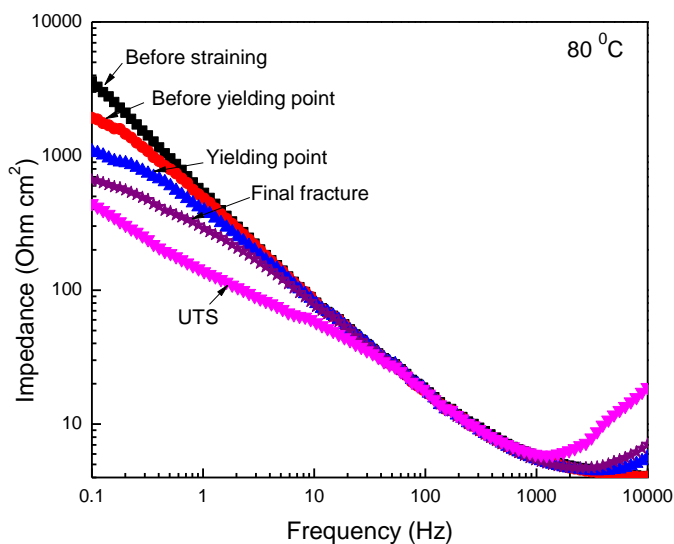


**Figure 10.** Bode plot in the Impedance-frequency format for UNS S41425 supermartensitic stainless steel in H<sub>2</sub>S-containing 3.5 % NaCl solution at 80 °C during the SSRT.

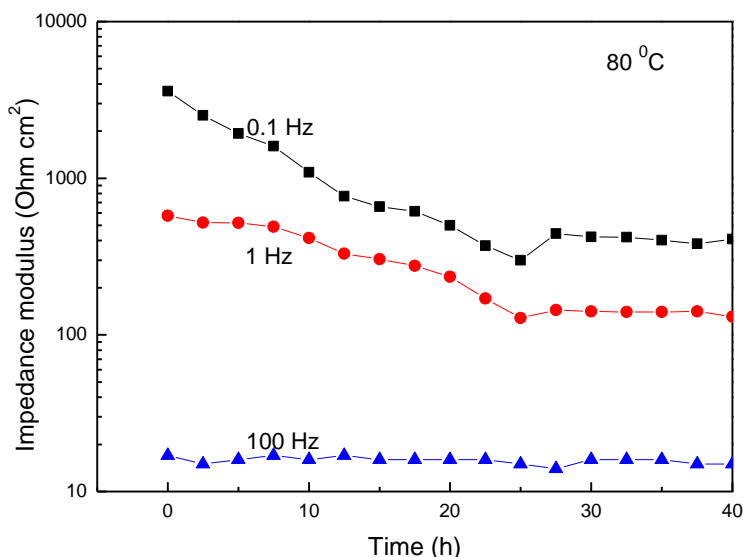


**Figure 11.** Evolution of the impedance modulus with time at different frequencies for UNS S41425 supermartensitic stainless steel in H<sub>2</sub>S-containing 3.5 % NaCl solution at 80°C during the SSRT.

Specimen fractured at 80 °C increased its susceptibility towards SCC, as indicated data from Fig. 2. Nyquist diagram for unstressed specimen, Fig. 9, displayed, what looks like an unfinished semicircle with its centre at the real axis; as soon as the specimen was strained, data displayed a semicircle at high and intermediate frequencies, together with a second loop at lower frequency values. One of the observed loops in Fig. 9 corresponds to the formed sulfide film, whereas the second loop corresponds to the double electrochemical layer. It can be seen that as the specimen was strained and time elapsed, the semicircle diameter decreased except at the final fractured, where the semicircle diameter increased again. Additionally, as time elapsed, data displayed only one semicircle, which might be due to the crack opening and growth and the degradation of the external sulfide film due to the applied stress. This is reflected in the Bode-modulus plot, Fig. 10, the total impedance at the lowest frequency increased as time elapsed, indicating the external sulfide film degradation and crack growth. The change in the impedance modulus with time at different frequency values is plotted in Fig. 11, where it can be seen that at 100 Hz, this parameter remained practically constant as time elapsed. However, at lower frequency values, i.e. 1 and 0.1 Hz, the impedance modulus decreased as the applied stress increased, just as reported by Oskuie and Bosch [24,25] and related this fact to an increase in the crack size and/or in the number of secondary cracks.

The Bode-phase angle plot, practically remained constant with time in a frequency window of 10-1000 Hz or so, Fig. 12; for frequency values lower than 10 Hz, the phase angle decreased as the specimen was strained, except when it reached the final rupture, where the angle phase increased again. Thus, Fig. 13 shows that at 100 and 1000 Hz, the phase angle remained more or less constant during the straining, but at 1 Hz, the phase angle decreased as the specimen was strained. In all cases

the phase angle increased once the specimen was ruptured, which might be due to repassivation and film growth on the crack corroded surface [25]. Such a decrease in phase angle can be correlated to the corrosion cracking process, as reported elsewhere [24, 26, 34, 35] for instance, for the SCC of carbon steel in fuel-grade ethanol.

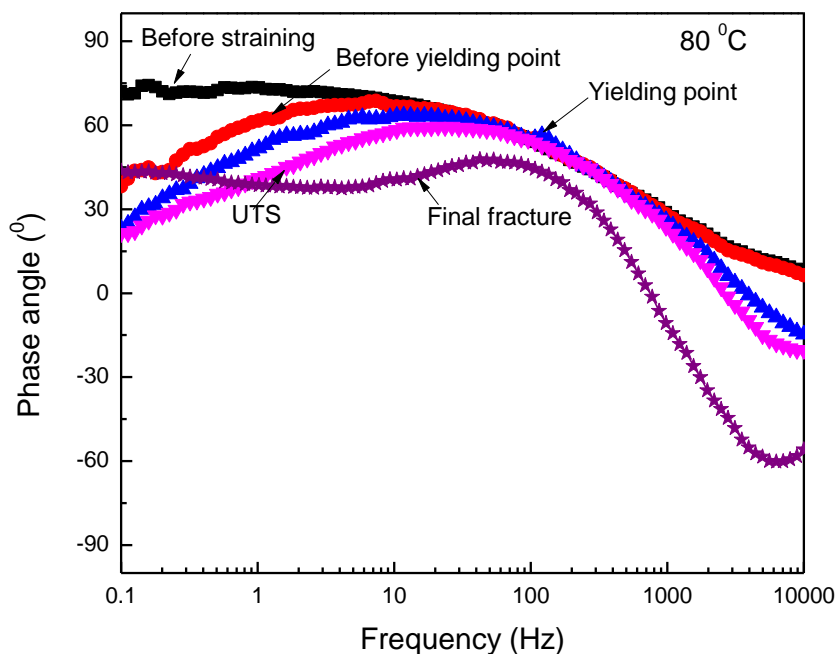


**Figure 12.** Bode curve in the Phase angle-frequency format for UNS S41425 supermartensitic stainless steel in  $H_2S$ -containing 3.5 % NaCl solution at  $80\text{ }^\circ\text{C}$  during the SSRT.

In Fig. 13 it can be seen that at higher frequencies than 1000 Hz, the phase angle remained constant as time elapsed, but at 100 and specially 1 Hz, the phase angle decreased after 10 hours, as the steel was strained. It can be seen from Figs. 5 and 10 that at 0.1 Hz, the decrease in both the impedance modulus and the angle phase changes in slope after 20 hours more or less, once necking has started [32] which can be an indicator of passive layer deterioration in the necking area on the gauge of the tensile specimen. This effect has been related by Oskuie, Bosch and Lou [24-26] to an increase in the crack size. Here, once again, these results are consistent with the reported results by other researchers [24, 25] who have reported that cracks can only be detected at frequencies lower than 10 Hz, which the authors proposed as the suitable frequency range for detection of the cracks.

In order to interpret its EIS response during a stress corrosion crack, many factors can be involved such as crack tip behavior, crack wall behavior, solution chemistry in the crack, and crack propagation path. For the interpretation of the EIS data, it is a common practice to use Randles circuit (Fig. 14) where  $R_{sol}$ ,  $R_w$ ,  $R_{ct}$  and  $C_{dl}$  are the solution resistance, the resistance of a Warburg's element, charge transfer resistance and double layer capacitance respectively. However, in our experiments,

SCC is a dynamic process which involves changes in both crack geometry and electrochemical activity. These changes are contributed by crack growth, crack tip activity, crack wall activity including secondary cracks growth, and crack chemistry inside a single crack. Inside the crack,  $R_w$  represents the resistance of the Warburg element or a diffusion layer.

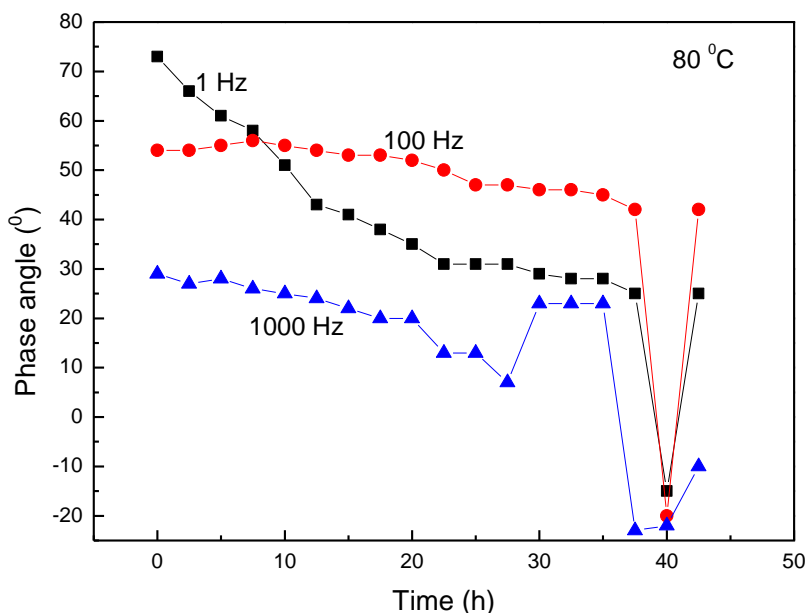


**Figure 13.** Evolution of the phase angle with time at different frequencies for UNS S41425 supermartensitic stainless steel in  $H_2S$ -containing 3.5 % NaCl solution at 80 °C during the SSRT.

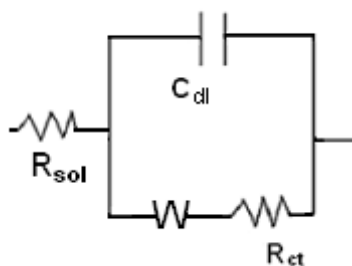


**Figure 14.** Electric circuit used to simulate EIS data at 80 °C.

Since stress corrosion cracking is a dynamic process, this should be reflected within the interval of used frequencies during the EIS experiments. The response from a higher frequency perturbation represents a faster electrochemical process, which is more close to a non-Faradaic process. The presence of a diffusional Warburg impedance in the EIS should be associated to surface concentration of an electrochemical active species changes during the AC cycle, and reflects in for example, the impedance of the cathodic reaction. At high frequencies the real and imaginary parts of the impedance

are equal for semi-infinite diffusion. Thus, our results show that there is a frequency lower than 1 Hz where the electrochemical behavior after the maximum stress is very clear. The frequency interval between 1 and 0.1 Hz represents at the best the cracking behavior in a reasonable way.

**Table 2.** Parameters used to simulate the EIS data at 60 °C using circuit in Fig. 17

Point	$R_{sol}$ (Ohm cm <sup>2</sup> )	$R_w$ (Ohm cm <sup>2</sup> )	$C_{dl}$ (μF cm <sup>-2</sup> )	n	$R_{ct}$ (Ohm cm <sup>2</sup> )
Before straining	4.42	3685	15.8	0.73	70
Before yielding point	3.94	8610	24.8	0.81	435
Yielding point	3.71	12735	15	0.86	631
UTS	3.78	501	95	0.76	450
After rupture	4.45	3053	14.7	0.86	10

The changes in the shape of the Warburg impedance can be associated to the form of the pore or crack which affects the AC signal penetration within the crack [41]. Table 2 shows the parameters used to simulate the obtained EIS data for test performed at 80 °C. It can be seen that both the resistance of the diffusion layer inside the crack,  $R_w$  and the charge transfer resistance,  $R_{ct}$ , are the parameters which are greatly modified during the straining. Thus, It can be seen that, generally speaking, both  $R_w$  and  $R_{ct}$  increased with time, reaching its highest value at the yielding point, decreased at the UTS, and increased once again at the final rupture. This means that the aggressive species diffuse more easily through this layer after the yielding point; at final rupture the  $R_w$  value increased once again, maybe because the crack walls are repassivated making more difficult the access of the aggressive species. However, the  $R_w$  values were higher than those for  $R_{ct}$ , indicating a diffusion-controlled process. In the literature, there are studies of the effect of H<sub>2</sub>S on iron and steel [37-40]. These results showed that both the anodic iron dissolution and the cathodic hydrogen evolution are accelerated by H<sub>2</sub>S. Sulfide-induced SCC is a process enhanced by an anodic dissolution process, where the access of the aggressive species including hydrogen cathodic discharge is necessary for corrosion to occur, which is in agreement with the results found in this study.

#### 4. CONCLUSIONS

Electrochemical impedance spectroscopy (EIS) has been used to study the initiation and propagation of sulfide stress corrosion cracks (SSCC) in a supermartensitic stainless steel by using the slow strain rate tests. It was found that when the steel is susceptible to SSCC both the Bode modulus and phase angle decreased as straining increased in a frequency interval of 0.1 and 10 Hz. Unlike this, when the steel was immune to SSCC no change in neither the Bode modulus and phase angle was detected. Equivalent electric circuit has been proposed to simulate the EIS data and it was found that the resistance of a diffusion layer inside the crack, and its charge transfer resistance decreased after the yielding point, enhancing, thus, the corrosion within the crack.

## References

1. A. John Sedriks, "Corrosion of Stainless Steels", John Wiley and Sons, Inc., Princeton, NJ, 1979.
2. T. Taira, K. Tsukada, Y. Kobayashi, H. Inagaki and T. Watanabe, *Corrosion* 37 (1981) 5.
3. H. Pircher and G. Sussek, *Corros. Sci.* 27 (1987) 1183.
4. G. Domizzi, G. Anteri and J. Ovejero-García, *Corros. Sci.* 43 (2001) 325.
5. L.W. Tsay, M.Y. Chi, H.R. Chen and C. Chen, *Mater. Sci. Eng.* 416 A(2006) 155.
6. The Institute of Materials, *Corrosion Resistant Alloys for Oil and Gas Production: Guidance on General Requirements and Test Methods for H<sub>2</sub>S Service*, Maney publishing, (2002) p. 9.
7. H. Marchebois, J. Leyer, B. Orlans-Joliet, Proceedings from the NACE Corrosion conference (2007), Paper 07090 2007 CP, Houston, TX, NACE International.
8. X. Li, T. Bell, *Corros. Sci.* 48 (2006) 2036.
9. M.D. Pereda, C.A. Gervasi, C.L. Llorente and P.D. Bilmes, *Corros. Sci.* 53 (2011) 3934.
10. H. Van-der-Winden, P. Toussaint and L. Coudreuse, Proceedings, Past, Present and Future of Weldable Supermartensitic Alloys, Supermartensitic Stainless Steel, Brussels, Belgium, 2002.
11. T.G. Gooch, P. Woollin and A.G. Haynes, Proceedings, Welding Metallurgy of Low Carbon 13% Chromium Martensitic Steels, Supermartensitic Stainless Steel, Brussels, Belgium, 1999.
12. D. Carrouge, Proceedings, Transformations in supermartensitic stainless steels", Ph.D. thesis, University of Cambridge, Department of Materials Science and Metallurgy, England, 2002.
13. S. Ritter and H. P. Seifert, *Materials and Corrosion* 64 (2013) 683.
14. R.C. Rathod, S.G. Sapate, R. Raman and W.S. Rathod, *J. Mat. Eng. and Perf.* 22 (2013) 3801.
15. Mathias Breimesser, Stefan Ritter, Hans-Peter Seifert, Thomas Suter, and Sannakaisa Virtanen, *Corr. Sci.* 63 (2012) 129.
16. C.J. Ortiz Alonso, M.A. Lucio-Garcia, I.A. Hermoso-Diaz, J.G. Chacon-Nava, A. MARTINEZVILLAFañE and J.G. Gonzalez-Rodriguez, *Int. J. Electrochem. Sci.*, 9 (2014) 6717.
17. Li Jian, Kong Weikang, Shi Jiangbo, Wang Ke, Wang Weikui, Zhao Weipu and Zeng Zhoumo, *Int. J. Electrochem. Sci.*, 8 (2013) 2365.
18. G.L. Edgemon, M.J. Danielson and G.E.C. Bell, *J. Nuclear Materials* 245 (1997) 201.
19. J. Hickling, D.F. Taylor and P.L. Andresen, *Materials and Corrosion* 49 (1998) 651.
20. J. Kovac, M. Leban and A. Legat, *Electrochim. Acta* 52 (2007) 7607.
21. T. Anita, M.G. Pujar, H. Shaikh, R.K. Dayal and H.S. Khatak, *Corros. Sci.* 48 (2006) 2689.
22. G. Du, J. Li, W.K. Wang, C. Jiang and S.Z. Song, *Corros. Sci.* 53 (2011) 2918.
23. S.W. Kim and H.P. Kim, *Corros. Sci.* 51 (2009) 191.
24. A.A. Oskuie, T. Shahrabi, A. Shahriari and E. Saebnoori, *Corros. Sci.* 61 (2012) 111.
25. Rik-Wouter Bosch, *Corros. Sci.* 47 (2005) 125.
26. Xiaoyuan Lou and Preet M. Singh, *Electrochim. Acta* 56 (2011) 1835.
27. S. Arzola, J. Mendoza-Florez, R. Duran-Romero and J. Genesca, *J. Solid. State. Electrochem.* 7(2003) 283.
28. T.A. Ramanarayanan and S.N. Smith, *Corrosion* 46 (1990) 66.
29. H. Vedage, T.A. Ramanarayanan, J. D. Mumford and S.N. Smith, *Corrosion* 49 (1993) 114.
30. Pengpeng Bai, Shuqi Zheng, Hui Zhao, Yu Ding, Jian Wu and Changfeng Chen, *Corros. Sci.* 87 (2014) 397.
31. H. Amaya, K. Kondo, H. Hirata, M. Ueda and T. Mori, Proceedings from the NACE Corrosion conference 1998, Paper 98113, 1998,CP, Houston, TX, NACE International.
32. M. Salazar, M. A. Espinosa-Medina, P. Hernández and A. Contreras, *Corros. Eng. Sci. and Tech.* 46 (2011) 464.
33. H. Keiser, K.D. Beccu and M.A. Gutjahr, *Electrochim. Acta* 21 (1976) 539.
34. R.W. Bosch, F. Moons, J.H. Zheng and W.F. Bogaerts, *Corrosion* 57 (2001) 532.
35. M.C. Petit, M. Cid, M. Puiggali and Z. Amor, *Corros. Sci.* 31 (1990) 491.
36. R. de Levie, *Adv. Electrochem. Eng.* 6 (1967) 329.

37. H.Y. Ma, X.L. Cheng, S.H. Chen, C. Wang, J.P. Zhang and H.Q. Yang, *J. Electroanal. Chem.* 451 (1998) 11.
38. M.A. Veloz and I. González, *Electrochim. Acta*, 48 (2002) 135.
39. 18. H.H. Huang, J.T. Lee and W.T. Tsai, *Mater. Chem. Phys.* 58 (1999) 177.
40. S. Arzola and J. Genesca, *J. Solid State Electrochem.* 8 (2005) 197.
41. D. D. Macdonald, *Electrochim. Acta.* 51 (2006) 1376.

© 2015 The Authors. Published by ESG ([www.electrochemsci.org](http://www.electrochemsci.org)). This article is an open access article distributed under the terms and conditions of the Creative Commons Attribution license (<http://creativecommons.org/licenses/by/4.0/>).